Electronic Supplementary Material (ESI) for Physical Chemistry Chemical Physics.

Nitrogen rejection in natural gas using NaZSM-25 zeolite

Seyed Hesam Mousavi,[a] Javad Tamnanloo,[b] Abdol Hadi Mokarizadeh,[b] Ali Zavabeti,[a] Jefferson Zhe Liu,[*c] Gang Kevin Li[*a].

[a] Department of Chemical Engineering, The University of Melbourne, Parkville, Victoria 3010, Australia, Email: li.g@unimelb.edu.au

[b] School of Polymer Science and Polymer Engineering, University of Akron, Akron, Ohio 44325, United States,

[c] Department of Mechanical Engineering, The University of Melbourne, Parkville, Victoria, 3010, Australia, Email: zhe.liu@unimelb.edu.au

Supporting Information

1. Supplementary text

S1. Langmuir isotherm model

A four-parameter Langmuir isotherm model[1] was fitted to describe the uptake of N_2 and CH_4 as follows:

$$Q_i = \frac{IP_{1i} e^{IP_{2i}/T} P_i}{1 + IP_{3i} e^{IP_{4i}/T} P_i} \quad (1)$$

Where, Q_i is the equilibrium gas loading of component *i* [kmol/$kg_{adsorbent}$] and IP_{1i} *to* IP_{4i} are model parameters for component *i* with units of [kmol/$kg_{adsorbent}$/bar], [K], [bar^{-1}], and [K], respectively. P_i is the equilibrium pressure of component *i* [bar], *and T* is the adsorption temperature [K].

S2. Clausius-Clapeyron equation

The Clausius-Clapeyron equation[2] was used to estimate isosteric heats of adsorption (Q_{st}) based on the isotherms obtained at 313 and 323 K.

$$Q_{st} = RT^2 \left(\frac{\partial \ln P}{\partial T}\right)_q \quad (2)$$

where, R is the gas constant [J mol^{-1} K^{-1}], *T* is the temperature [K], and *P* is the pressure for given quantity of gas adsorbed (n) [bar].

S3. Simulation in Aspen Adsorption

A commercial software called Aspen Adsorption was used for simulation of breakthrough curves. It solves mass, momentum, and energy conservation equations for a vertical adsorption bed by generating a set of differential and algebraic equations for evenly spaced points over the length of the bed. First-order Upwind Differencing Scheme 1 (UDS1) with 20 nodes was used as the discretization method and Implicit Euler as the solving method. . The major

assumption in this simulation was that the column operates isothermally. Other assumptions are discussed in the following sections.

S3.1. Mass Balance

Eq. 3 shows the general mass balance equation in gas phase for each component along the radial and vertical axes of the adsorption bed.

$$\varepsilon_B \frac{\partial c_i}{\partial t} + \frac{\partial (c_i v_g)}{\partial z} + \rho_s \frac{\partial q_i}{\partial t} - \varepsilon E_{zi} \frac{\partial^2 c_i}{\partial z^2} - \varepsilon E_{ri} \frac{1}{r} \frac{\partial}{\partial r} \left(\frac{\partial^2 c_i}{\partial r} \right) = 0 \qquad (3)$$

where c_i = concentration of component *i* in the gas phase (kmol/kg), *t* = time (s), v_g = superficial gas velocity (m/s), ρ_s = adsorbent bulk density (kg/m^3), q_i = adsorbent gas loading (kmol/kg$_{adsorbent}$), ε = interparticle porosity, ε_B = bed porosity, E_{zi} = axial dispersion coefficient of component *i* (m^2/s), *z* = differential length of the adsorption column (m), and E_{ri} = radial dispersion coefficient of component *i* (m^2/s).

To simplify the equation furthermore, the following assumptions were made:

- Radial gradients being considerably smaller that the axial gradients, were neglected. Thus, assuming a one-directional gas flow, the last term of Eq. 3 can be ignored.
- Compared to forced mass transfer, axial dispersion effects in overall mass transfer can be neglected.[2-6] Hence, the second to last term of Eq. 3 can be ignored.
- Peng-Robinson equation was used as the equation of state for gas phase to describe pressure, volume, and temperature relationship.
- Eq. 4 shows the linear driving force model with lumped mass transfer coefficient that was used for describing gas uptake rate.[4, 7, 8]

$$\frac{\partial q_i}{\partial t} = k_i (q_i^* - q_i) \qquad (4)$$

where q_i^* = equilibrium gas loading of component i (kmol/kg) and k_i = mass transfer coefficient of component *i* (s^{-1}).

Eq. 5 shows the simplified mass balance equation. The remaining terms describe accumulation in gas phase, convection, and accumulation in solid phase respectively.

$$\varepsilon_B \frac{\partial c_i}{\partial t} + \frac{\partial (c_i v_g)}{\partial z} + \rho_s \frac{\partial q_i}{\partial t} = 0 \quad (5)$$

where ε_B = bed porosity, c_i = concentration of component *i* in the gas phase (kmol/kg), *t* = time (s), v_g = superficial gas velocity (m/s), *z* = differential length of the adsorption column (m), ρ_s= adsorbent bulk density (kg/m^3), and q_i = gas loading (kmol/kg).

S3.2. Momentum Balance

The pressure drop along the bed was estimated by Ergun equation, as it is valid for a wide range of flow regimes[1, 2, 6] (Eq. 6)

$$\frac{\partial P}{\partial z} = -[\frac{1.5 \times 10^{-3}(1-\varepsilon)^2}{\left(2r_p\psi\right)^2 \varepsilon^3}\mu_g v_g + 1.75 \times 10^{-5} Mw \rho_g \frac{(1-\varepsilon)}{2r_p\psi\varepsilon^3} v_g^2] \quad (6)$$

where μ = dynamic viscosity (Ns/m^2), r_p= particle radius (m), ψ= particle sphericity, μ_g= gas phase viscosity (Pa·s), *M* = gas molecular weight (kg/kmol) and ρ_g = gas phase density (kg/m^3).

S4. Breakthrough simulation

We employed breakthrough simulation as a substitute for experimental breakthrough due to the following limitations:

First, the adsorption kinetics in our study were found to be relatively slow, with a mass transfer coefficient of N_2 measured at 0.0031 s^{-1}. This indicates that in order to achieve noticeable adsorption, detention times of several hundred seconds are required.

Secondly, the amount of absorbent used was insufficient. To satisfy the mentioned detention time (1000 s), we needed to decrease the flow rate to less than 0.1 ml/min to reach the mentioned detention time with the available amount of the adsorbent.

$$F = \frac{\frac{Mass}{Density}}{Detention\ time} = \frac{\left(\frac{1\ g}{0.604\ \frac{g}{cm^3}}\right)}{1000\ s} = 0.00165\ \frac{ml}{s} = 0.1\frac{ml}{min} \quad (7)$$

Subsequently, it was necessary to maintain Péclet numbers above 100 to mitigate the axial dispersion effect. The Péclet number is a dimensionless quantity that represents the ratio of advection to diffusion. In mass transfer context, $Pe = uL/D$ where u is the gas velocity, L is the bed length, and D is the diffusion coefficient. Velocity can be calculated by dividing flowrate by bed sectional area $u = F/A$, therefore $Pe = \frac{\frac{F}{A}*L}{D}$ and $\frac{L}{A} = \frac{Pe * D}{F}$. Using $D \approx 0.2\frac{cm^2}{s}$, $F = 0.00165\frac{cm^3}{s}$, and $Pe \geq 100$, L/A must be at least 12000 cm^{-1}. This means that the bed must have a cross section area of 0.0117 cm^2 and length of 140 cm.

Hence, we utilized the ASPEN Adsorption simulation software to design a significantly larger bed comprising over 500 g of adsorbent. Synthesizing such a substantial quantity of adsorbent was unfeasible within the limitations of our laboratory-scale synthesis equipment.

The breakthrough separation was simulated by Aspen Adsorption V10 with binary mixtures of CH_4/N_2 (50/50) flowing at 50 mL/min at 300 K. Dimensions of a lab-scale experimental rig was used for the simulation. The Aspen adsorption flow sheet for simulating dynamic breakthrough experiments is shown in Figure S1. Using an isothermal model, Aspen Adsorption solved spatially discretized equations to simulate the breakthrough curves of CH_4 and N_2. The properties of adsorbent and adsorption bed characteristics were given in Tables S1-S2.

Equilibrium behaviour of the gas-solid interactions was described by the Langmuir model (Eq. 1). Parameters of the model fitted experimentally with good agreement and they are listed in Table S2.

S5. Replica exchange Monte Carlo and molecular dynamic simulations

The experimentally obtained crystal structure of the MWF framework was used as the unit cell in the atomistic simulations. Lattice parameters of the unit cell and its pristine composition are shown in Table S3.

Throughout the simulation, it is assumed that the simulated cell dimension remains unchanged which is close to reality. Due to the size of the unit cell and to avoid time-consuming computation, a single unit cell is used without replication. The simulation box is periodic in every three dimensions of X, Y, and Z directions. For adding Na^+ cations to the unit cell, 270 atoms of Si were replaced with Al randomly avoiding Al-O-Al linkage, according to Lowenstein's rule. The final structure with a composition of $O_{2880}Al_{270}Si_{1170}Na_{270}$ holds the ratio of Si/Al ~ 4.33.

All atomistic simulations were performed in the RASPA[9, 10] package. All needed interatomic parameters were adopted from the forcefield proposed by Boulfelfel et al.[11] and reported in Tables S4 and S5. Ewald summation is used to describe long-range interactions with an accuracy of 10^{-6}. The cut-off distance was set to 12.0 Angstrom.

Replica exchange Monte Carlo was used for finding the equilibrium position of Na^+ cations in the structure. Parallel tempering ensures an enhancement in the sampling of the lower energy states. Eight replicas of the system containing 270 Na^+ cations in a single unit cell were simulated simultaneously with T= 300, 390, 507, 857, 1114, 1448, 1882, and 2447 K. Highest temperature for the last replica was chosen in a way that ions could move freely in the pores. Each replica was simulated with more than 21×10^6 Monte Carlo moves to ensure that system was equilibrated as well as well sampled. Cations were let to translate and replica-exchange moves throughout the simulation with probabilities of 1.0 and 0.1, respectively.

Further investigation of the pore-blocking effect by the cations was performed by molecular dynamics. 50 N_2 or CH_4 molecules randomly distributed in the NaZSM-25. All atoms of the silica structure were kept fixed while cations and gas molecules were able to move in the corresponding unit cell structure. Each system was simulated for 100 picoseconds with a timestep of 1.0 femtosecond in NVT ensemble.

S6. Density functional theory (DFT) calculations

Diffusion-associated energy barriers as well as trajectories of gas molecules and door-keeping cations in NaZSM-25 were estimated using *Ab initio* DFT calculations. The Vienna *Ab initio* Simulation Package[12] was employed with the projector augmented waves approach[13] and the dispersion-corrected DFT-D3 functional[14].

The cut-off energy of the plane wave basis-set for all DFT calculations was 405 eV. A gamma point only k-point mesh was applied to the 8MR cluster of NaZSM-25. The mentioned values for cut-off energy and k-point mesh ensured us that the convergence error of the total energy will be smaller than 1 meV/atom. The van der Waals interactions were estimated by the DFT-D3 functional (with IVDW=11). The conjugate gradient method with a threshold of 0.015 eV/Å for the forces acting on atoms was employed to optimize the position of atoms, as suggested by Göltl and Hafner.[15]

We extracted the 8MR from the unit cell of the ZSM-25 as the cluster to be studied. The lattice parameters of the unit cell were a=b=c=25 Å and α=β=γ=90.0°. To rectify the dangling bonds, we saturated the cluster's boundary O atoms with H atoms by locating them at 1 Å distance and further relaxation of the whole cluster.

Then, we relaxed a Na^+ cation inside the 8MR to find the optimum position of the cation. To find the diffusion energy barrier, we used the nudged elastic band (NEB) method as implemented in VASP code. We placed the gas molecules on each side of the 8MR and created trajectory images to force the gas molecule to pass the ring. By comparing the energy level of the trajectory images, we obtained the $\Delta E_{barrier\text{-}gas}$.

2. Supplementary figures

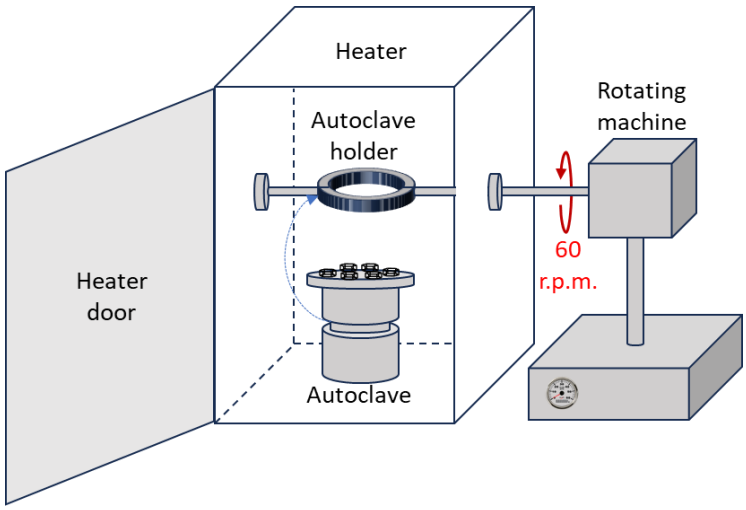

Figure S1. Schematic diagram of the experimental rotating autoclave-heater system for synthesis crystallization step.

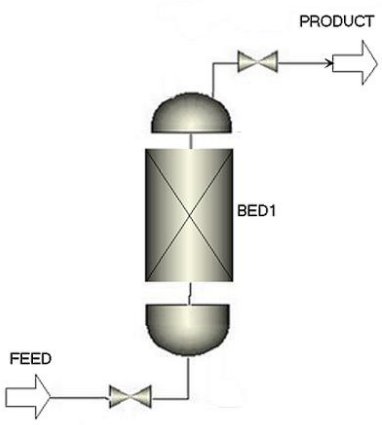

Figure S2. The flowsheet of the breakthrough simulation in Aspen Adsorption.

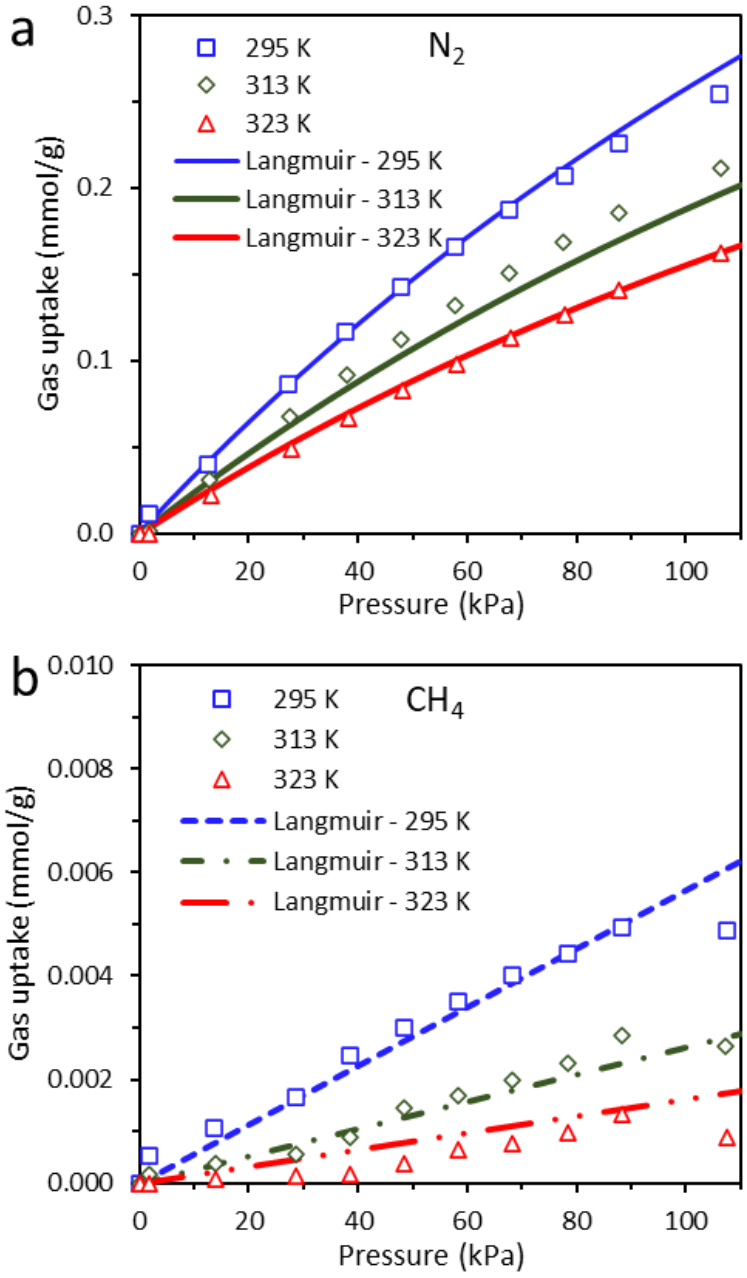

Figure S3. Langmuir isotherm fitting results for N_2 (a) and CH_4 (b) at 295, 313, and 323 K.

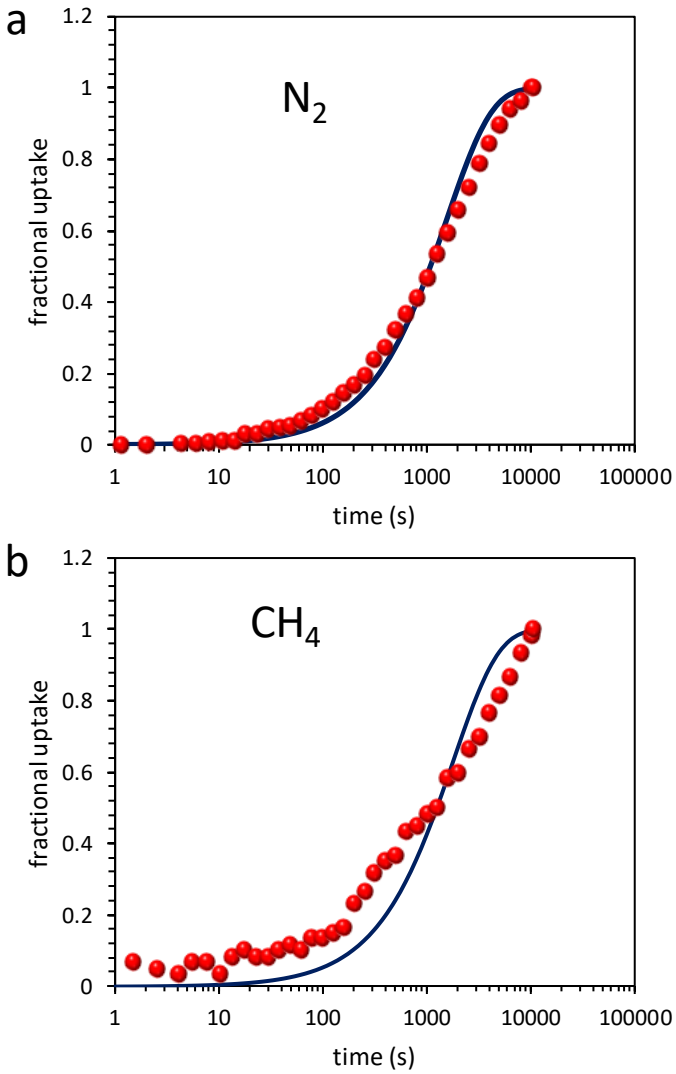

Figure S4. Linear driving force model fitting on rate of adsorption measurement results for N_2 (a) and CH_4 (b) at 295 K for pressure change between 50-100 kPa.

Supplementary tables

Table S1. Properties of NaZSM-25 sample, and parameters of packed bed used for breakthrough simulation.

Parameter	Value	Unit	Description
H_b	0.5	m	Height of adsorbent bed
D_b	0.05	m	Internal diameter of adsorbent bed
E_i	0.43	m^3 void/m^3 bed	Inter-particle porosity
E_p	0.549	m^3 void/m^3 bead	Intra-particle porosity
RHO_s	604.8	kg/m^3	Bulk density
R_p	$1.5e^{-4}$	m	Adsorbent particle radius
S_{Fac}	1	n/a	Adsorbent shape factor

Table. S2 Mass transfer coefficient of the Linear Driving Force model and parameters of the Langmuir isotherm model

Parameter	Value	Unit	Description
MTC("CH_4")	0.0158	s^{-1}	Mass transfer coefficients
MTC("HELIU-01")	0	s^{-1}	Mass transfer coefficients
MTC("N_2")	0.0031	s^{-1}	Mass transfer coefficients
IP(1,"CH_4")	5.87E-13	kmol/kg/bar	Isotherm parameter
IP(1,"HELIU-01")	0	kmol/kg/bar	Isotherm parameter
IP(1,"N_2")	4.79E-07	kmol/kg/bar	Isotherm parameter
IP(2,"CH_4")	4796.28	K	Isotherm parameter
IP(2,"HELIU-01")	0	K	Isotherm parameter
IP(2,"N_2")	1959.09	K	Isotherm parameter
IP(3,"CH_4")	0.00764696	bar^{-1}	Isotherm parameter
IP(3,"HELIU-01")	0	bar^{-1}	Isotherm parameter
IP(3,"N_2")	0.307145	bar^{-1}	Isotherm parameter
IP(4,"CH_4")	0.046599	K	Isotherm parameter
IP(4,"HELIU-01")	0	K	Isotherm parameter
IP(4,"N_2")	20.1973	K	Isotherm parameter

Table S3. Lattice parameters of the unit cell and its pristine composition

Unit cell parameter	Value	Unit
a	44.924	Å
b	44.924	Å
c	44.924	Å
α	90	degree
β	90	degree
γ	90	degree
Volume	89581	$Å^3$
Composition	$O_{2880}Si_{1440}$	-

Table S4. The force field parameters for cation-framework interactions obtained from Boulfelfel et al[11].

Cross-Species	A (10^4 K)	B (Å^{-1})	C (10^3 K×Å^6)
Na – O_z	5581	3.985	917
Species	Charge (e)		
Si	1.8708		
Al	1.7906		
O	-0.9354		
Oa	-1.1427		
Na	0.9094		

Table S5. The force field parameters for adsorbate-adsorbate and adsorbate-adsorbent interactions obtained from Boulfelfel et al[11].

Cross-Species	ε (K)	σ (Å)	Species	Charge (e)
			N_2	
N_N_2 – Oz (Oa)	25.8	3.213	N_N_2	-0.40484
N_N_2 – Si	43.5	3.652	N_com	0.80968
N_N_2 – Al	55.4	3.067		
N_N_2 – Li	601.9	2.093		
N_N_2 – Na	117.2	2.567		
N_N_2 – K	153.2	3.068		
N_N_2 – Rb	157.7	3.221		
N_N_2 – Cs	137.4	3.41		
N_N_2 – N_N_2	36.4	3.32		
			CH_4	
C_CH_4 – Oz (Oa)	20.6	3.378	C_CH_4	-0.24
C_CH_4 – Si	35.1	3.83	H_CH_4	0.06
C_CH_4 – Al	76.4	3.252		
C_CH_4 – Li	366	2.029		
C_CH_4 – Na	158.3	2.731		
C_CH_4 – K	72.4	3.277		
C_CH_4 – Rb	89.3	3.419		
C_CH_4 – Cs	111.5	3.541		
H_CH_4 – Oz (Oa)	16.7	2.833		
H_CH_4 - Si	25	3.285		
H_CH_4 – Al	55.7	2.777		
H_CH_4 – Li	389.2	1.628		
H_CH_4 – Na	140.7	2.256		
H_CH_4 – K	55.7	2.774		
H_CH_4 – Rb	65.3	2.918		
H_CH_4 – Cs	77.2	3.05		
C_CH_4 – C_CH_4	58	3.825		
H_CH_4 – H_CH_4	7.55	2.4		

References

1. R. I. Masel, *Principles of adsorption and reaction on solid surfaces*, John Wiley & Sons, 1996.
2. J. W. Yoon, H. Chang, S.-J. Lee, Y. K. Hwang, D.-Y. Hong, S.-K. Lee, J. S. Lee, S. Jang, T.-U. Yoon and K. Kwac, *Nature materials*, 2017, **16**, 526-531.
3. J. A. Delgado, M. A. Uguina, J. L. Sotelo, V. I. Águeda, A. Sanz and P. Gómez, *Computers & chemical engineering*, 2011, **35**, 1010-1019.
4. A. Ntiamoah, J. Ling, P. Xiao, P. A. Webley and Y. Zhai, *Adsorption*, 2015, **21**, 509-522.
5. A. Ntiamoah, J. Ling, P. Xiao, P. A. Webley and Y. Zhai, *Industrial & Engineering Chemistry Research*, 2016, **55**, 703-713.
6. C. Tian, Q. Fu, Z. Ding, Z. Han and D. Zhang, *Separation and Purification Technology*, 2017, **189**, 54-65.
7. C. Shen, Z. Liu, P. Li and J. Yu, *Industrial & Engineering Chemistry Research*, 2012, **51**, 5011-5021.
8. M. Xu, S. Chen, D.-K. Seo and S. Deng, *Chemical Engineering Journal*, 2019, **371**, 693-705.
9. D. Dubbeldam, S. Calero, D. E. Ellis and R. Q. Snurr, *Molecular Simulation*, 2016, **42**, 81-101.
10. D. Dubbeldam, A. Torres-Knoop and K. S. Walton, *Molecular Simulation*, 2013, **39**, 1253-1292.
11. S. E. Boulfelfel, J. M. Findley, H. Fang, A. S. Daou, P. I. Ravikovitch and D. S. Sholl, *The Journal of Physical Chemistry C*, 2021, **125**, 26832-26846.
12. G. Kresse and J. Furthmüller, *Physical review B*, 1996, **54**, 11169.
13. G. Kresse and D. Joubert, *Physical review b*, 1999, **59**, 1758.
14. S. Grimme, J. Antony, S. Ehrlich and H. Krieg, *The Journal of chemical physics*, 2010, **132**, 154104.
15. F. Göltl and J. Hafner, *The Journal of chemical physics*, 2011, **134**, 064102.